Evaluation of effectiveness of supervised classification algorithms in land cover classification using ASTER images-A case study from the Mankweng (Turfloop) Area and its environs, Limpopo Province, South Africa

Nndanduleni Muavhi

Department of Geology and Mining, University of Limpopo, Private Bag X1106, Sovenga, South Africa, nndandulenimuavhi@gmail.com

DOI: http://dx.doi.org/10.4314/sajg.v9i1.5

Abstract

The production of land cover maps using supervised classification algorithms is one of the most common applications of remote sensing. In this study, the effectiveness of supervised classification algorithms in land cover classification using ASTER data was evaluated in the Mankweng Area and its environs. The false colour composite image generated from combination of band 1, 2 and 3 in red, green and blue, respectively, was used to generate training classes for six land cover types (waterbody, forest, vegetation, Duiwelskloof leucogranite, Turfloop granite and built-up land). These were used to construct land cover maps using eight supervised classification algorithms: Maximum Likelihood, Minimum Distance, Support Vector Machine, Mahalanobis Distance, Parallelepiped, Neural Network, Spectral Angle Mapper and Spectral Information Divergence. To evaluate the effectiveness of the algorithms, the land cover maps were subjected to accuracy assessment to determine precision of the algorithms in accurately classifying the land cover types and level of confidence that can be attributed to the land cover maps. Most algorithms poorly performed in classifying spatially overlapping land cover types without abrupt boundaries. This indicates that the environmental conditions and distribution of land cover types can affect the performance of certain classification algorithms, and thus need to be considered prior to selection of algorithms. However, Support Vector Machine and Minimum Distance proved to be the two most effective algorithms as they provided better producer's and user's accuracy in the range of 80-100% for all land cover types, which represent good classification.

Keywords: *remote sensing; land cover types; supervised classification algorithms; accuracy assessment*

1. Introduction

Land cover is the material at the ground, such as vegetation, waterbody, soil, etc. (Comber et al., 2005). The production of land cover maps is one of the most common applications of remote sensing (Alrababah and Alhamad, 2006; Lobo et al., 2004). Land cover maps provide geographical information essential in fields such as biological conservation, environmental management and urban and rural planning (Jansen et al., 2008; Musaoglu et al., 2005; Fuller et al., 1998). The application of

remote sensing in land cover classification is based on the discrimination of earth's materials considering the difference that exists among their spectral properties (Whateley, 2006). The processing technique that allows for the identification of materials in an image according to their diagnostic spectral signatures is referred to as image classification (Richards and Jia, 2006). Supervised classification is the semi-automated technique that classifies pixels in an image into classes corresponding to user-defined training classes (Research Systems Inc, 2008). Training classes are groups of pixels that are selected as representative areas of land cover types that the user desires to map in the final output image (Richards and Jia, 2006). Supervised classification rests upon using proper algorithms to classify the pixels in an image as representing land cover types, and there is broad range of algorithms suitable for supervised classification of remotely sensed images (Richards and Jia, 2006).

Different remote sensors collect different data with various degrees of spatial and spectral resolutions. As a result, the number and kind of land cover types that can be identified in remotely sensed images can vary significantly depending on the sensors used to gather the images (Whateley, 2006). Since the launch of Landsat in the early 1970s, remotely sensed images have been widely used for land cover classification (NASA, 2013). However, with the launch of Advanced Spaceborne Thermal Emission and Reflection Radiometer (ASTER) in 1999, remotely sensed images with relatively better spectral and spatial resolutions became readily accessible and available (Whateley, 2006). ASTER is an advanced multispectral remote imaging instrument that covers a wide spectral region with 14 bands ranging from the visible to thermal infrared region with medium spatial resolution. The spatial resolution varies with spectral region: 15 m in Visible and Near-Infrared (VNIR), 30 m in the Shortwave-Infrared (SWIR), and 90 m in the Thermal Infrared (TIR). These three spectral regions have three, six, and five bands, respectively. Each ASTER scene has a swath width of 60 km (Whateley, 2006). ASTER images have been widely used for different purposes such as monitoring the rate of environmental changes, construction developments, agricultural activities and anthropogenic changes, and mapping of natural resources (Mohd et al., 2009; Bagan et al., 2008; Yuksel et al., 2008).

The aim of the present study was to evaluate the effectiveness of eight supervised classification algorithms: Maximum Likelihood, Minimum Distance, Mahalanobis Distance, Parallelepiped, Neural Network, Support Vector Machine, Spectral Angle Mapper and Spectral Information Divergence in land cover classification using ASTER data.

2. Study area

The study was conducted in the Mankweng (Turfloop) Area and its environs which is situated in the central part of Limpopo Province, South Africa. It is located approximately 10 km east of the Polokwane City. The study area also covers the University of Limpopo and Mankweng Hospital. The study area extends over an area of 60 km^2 (Fig. 1).

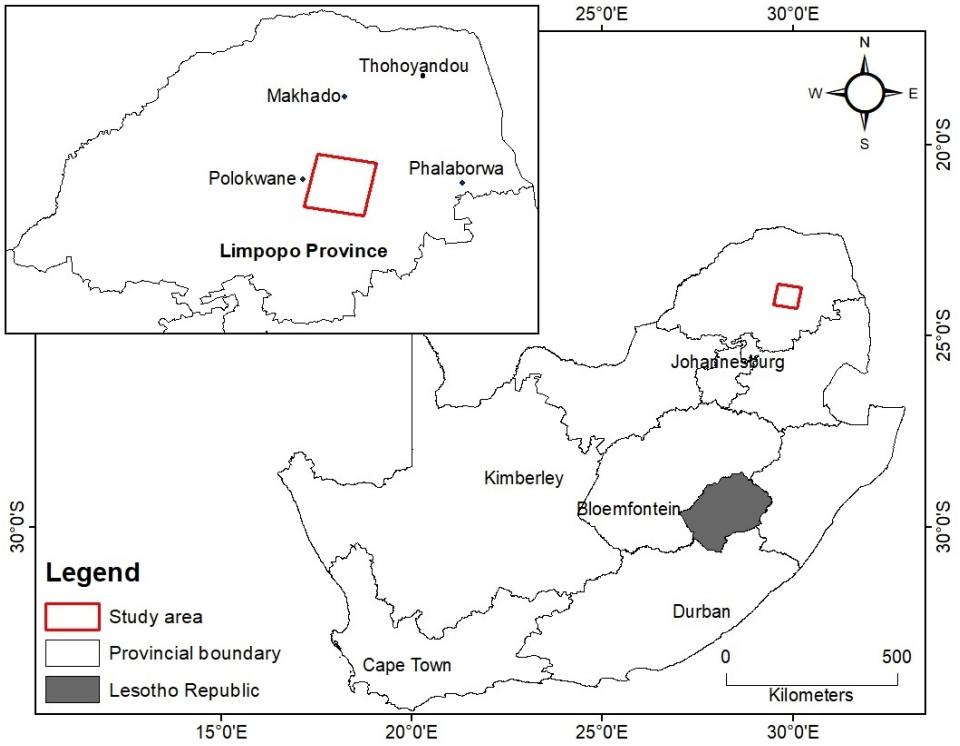

Figure 1: Locality map of the study area.

3. ASTER data

The ASTER data selected for this study is ASTER L1T (Precision Terrain Corrected Registered At-Sensor Radiance Product) cloud-free scene with Local Granule ID: AST_L1T_00310022003081250_20150501020734_95242, acquired on 02 October 2003. The ASTER L1T data product was retrieved on (https://lpdaac.usgs.gov) maintained by the NASA Land Processes Distributed Active Archive Center (LPDAAC) at the USGS/Earth Resources Observation and Science (EROS) Center, Sioux Falls, South Dakota. The ASTER scene's center is located at 23°57'52.56" latitude (South) and 29°51'40.68" longitude (East). The path and row of the scene is 169 and 77, respectively. Only the bands in VNIR spectral region were used in the present study (Table 1). The VNIR region was selected based on its spatial resolution (15 m) compared to SWIR (30 m) and TIR (90 m) spectral regions, which has significant impact on spatial details of land cover classification.

Table 1. Wavelength ranges, and spatial and radiometric resolutions of ASTER bands.

Spectral region	Band number	Wavelength range (µm)	Spatial resolution (m)
VNIR	1	0.52-0.60	15
	2	0.63-0.69	
	3N	0.78-0.86	

3.1. Pre-processing of ASTER data

The three VNIR bands were stacked together to build a new VNIR multiband image. The Log Residuals calibration was carried out on the multiband image. Log Residuals is used to remove solar irradiance, atmospheric transmittance, instrument gain, topographic effects, and albedo effects from radiance data. This calibration tool converts radiance data to a pseudo reflectance image which is useful in mapping land cover types (Green and Craig, 1985). Different band combinations were tested on Log Residuals-calibrated multiband image and displayed to create false color composite images to enhance information on land cover types. The false color composite image of band 1, 2 and 3 in red, green and blue, respectively, enhanced information of land cover types (Fig. 2) and was selected for further analysis.

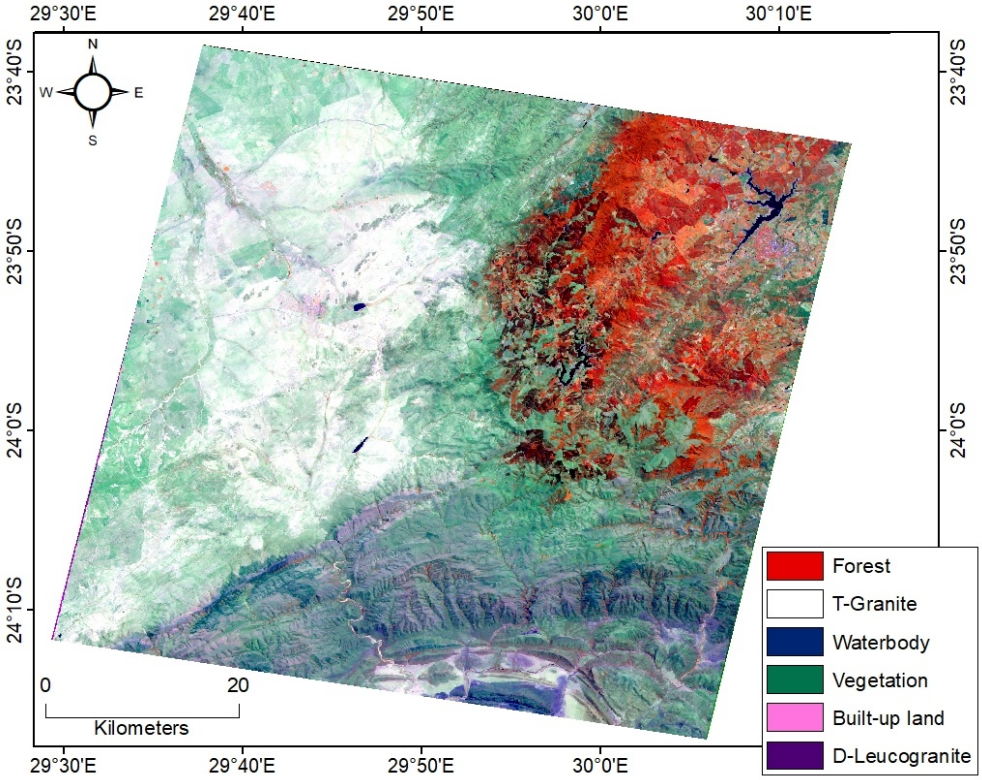

Figure 2: False color composite image showing land cover types.

3.2. Classification of ASTER images

The false colour composite image (Fig. 2), with the aid of geological map covering the study area (Robb et al., 2006), was thoroughly studied to identify pixels representing land cover types. Regions of interest (ROIs) for the land cover types were created and extracted from the false colour image to be used as training dataset for subsequent supervised classification using: Maximum Likelihood (ML), Minimum Distance (MD), Mahalanobis Distance (MhD), Parallelepiped (Pp), Neural Network (NN), Support Vector Machine (SVM), Spectral Angle Mapper (SAM) and Spectral Information Divergence (SID). The methodologies of these classification algorithms are explained in detail by

(Hsu et al., 2007; Richards and Jia, 2006; Du et al., 2004; Kruse et al., 1993). Table 2 shows the number of pixels used for individual training classes of land cover types characterizing the study area.

In this study, the objective was to classify all pixels in the Log Residuals-calibrated ASTER multiband image to specific land cover classes. Also, unclassified pixels create a void and affect interrelationship and interconnectedness that may exist among land cover classes in the ground resulting in an incomplete classification of image scene. For these reasons, the none threshold value option, which results in every pixel being assigned to the nearest land cover class for Maximum Likelihood, Minimum Distance and Mahalanobis Distance classifications, was selected. The none threshold option, resulted in the increased number of unclassified pixels for Parallelepiped classification. As a result, a single default maximum threshold value of 3.00 was used for Parallelepiped classification. Smaller angle and divergence measure values for Spectral Angle Mapper and Spectral Information Divergence, respectively, resulted in large number of unclassified pixels. To avoid decreased number of classified pixels, default maximum angle value (0.10) and divergence measure value (0.05) was selected for Spectral Angle Mapper and Spectral Information Divergence, respectively. For Support Vector Machine classification, the radial basis function kernel characterized by default gamma value of 0.33 and penalty parameter of 100.00, was used. The logistic activation method of Neural Network with default values of 0.90, 0.20, 0.90. 0.100, 1.00 and 1000.00 for training threshold contribution, training rate, training momentum, training RMS exit criteria, number of hidden layers and number of training iterations, respectively, was used to classify land cover types in the study area.

Table 2. Description of training classes used for supervised classifications.

Training class	Description	Pixel count
Forest	Evergreen forest, Nature Reserve	7179
Vegetation	Agricultural land, shrub and brush, grass and small trees	8668
Waterbody	Streams, lakes and dams	7923
D-leucogranite	Purplish to pinkish granitic rocks	8846
T-granite	Whitish granitic rocks/soils	466
Built-up land	Residential, public utilities, industrial and commercial complexes and roads	744

3.3. Accuracy assessment of classification

Accuracy assessment is a standard component of any land cover classification map derived from remotely sensed images. Accuracy is assessed empirically by checking the number of sample units assigned to each land cover type compared to the validation data also known as reference data or ground truth data. The validation data can be obtained by field visit or interpretation of photos, images or maps (Richards and Jia, 2006). Prior to selection of method of validation data gathering, the following key points were taken into consideration; (1) time and cost can affect the efficiency of collection of large validation data through field visit, and (2) the ASTER data used in the present study was acquired in 2003 and since there is a considerable difference of time between the acquisition date of ASTER data and the date of this manuscript writing, environmental changes and

construction developments might have occurred in the study area. For these reasons, interpretation of true colour satellite image from Google Earth Pro was used as validation data gathering tool. Google Earth Pro can revisit time and zoom in areas of interest at high resolutions; which the author deemed significant considering the acquisition date (October 2003) of the ASTER data used. The true colour image of the study area acquired in 2003 was thoroughly studied and regions of interest (ROIs) were extracted from the sites representing six land cover types. The extracted ROIs were examined for homogeneity and separability using n-D Visualizer. N-D Visualizer examines the separability of ROIs by looking at the distribution of the points within each ROI and looking for overlap between the land cover types. The points within ROIs for every land cover type should cluster together and not extensively overlap to other land cover types. The separability measures are reported as values ranging from 0-2 and indicate how well the ROIs separate. Values greater than 1.9 indicate that the ROIs pairs have excellent separability. Meanwhile, ROIs pairs with lower separability values can be improved by either editing the ROIs or selecting new ROIs (Richards and Jia, 2006).

At first attempts, Turfloop granite and built-up land ROIs pairs achieved low separability measures; and the true colour satellite image was used again to select new ROIs for these land cover types until their pairs attained better separability measures of 1.91. Other ROIs pairs achieved separability measures with values up to 2.00 (Table 3). Fig. 3 shows homogeneity and separability of ROIs and from the image the separability difficulty of Turfloop granite and built-up land is evident. The ROIs were used as validation classes for their respective land cover types. The number of pixels for every validation class is reported in Table 4.

Table 3. Separability values between land cover types pairs.

Land cover	Forest	Waterbody	Vegetation	D-leucogranite	T-granite	Built land
Forest		2.00	2.00	2.00	2.00	2.00
Waterbody	2.00		2.00	2.00	2.00	2.00
Vegetation	2.00	2.00		1.99	2.00	2.00
D-leucogranite	2.00	2.00	1.99		1.99	1.99
T-granite	2.00	2.00	2.00	1.99		1.91
Built-up land	2.00	2.00	2.00	1.99	1.91	

Table 4. Number of validation pixels for individual land cover types.

Validation class	Pixel count
Forest	3207
Vegetation	2497
Waterbody	2054
D-leucogranite	2488
T-granite	374
Built-up land	469

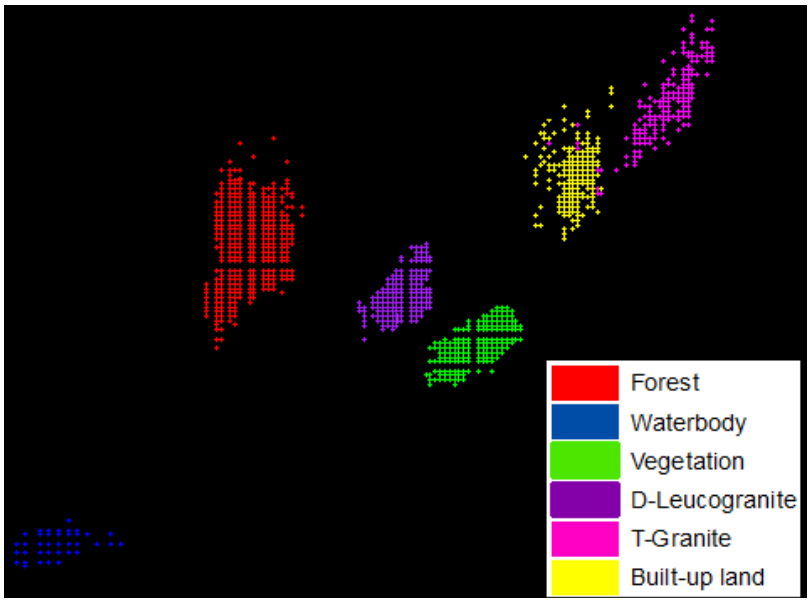

Figure 3: The n-D Visualizer image showing ROIs of the six land cover types.

The validation classes were used to assess the accuracy of the land cover maps using confusion matrix. In general, confusion matrix expresses the agreement of validation data and interpreted land cover types in the classification map (Richards and Jia, 2006). The most common accuracy measure is the overall accuracy, which is calculated by summing the number of validation pixels classified correctly for all land cover types and dividing by the total number of validation pixels of all land cover types. Another accuracy measure is the Kappa coefficient (K), which provides a difference measurement between observed agreement between training data and validation data and agreement occurring by chance alone (Jensen, 1986). Besides the overall accuracy and Kappa coefficient, the accuracy of individual land cover types can be calculated using producer's and user's accuracy, and commission and omission error. The producer's accuracy is the ratio of correctly classified validation pixels of a land cover type to total number of validation pixels of that land cover type; while, the user's accuracy can be defined as the ratio between correctly classified validation pixels for a land cover type to the total number of validation pixels classified as belonging to that land cover type. Commission error calculates the number of validation pixels misclassified as belonging to a land cover type while in the ground they represent other land cover types. On the other hand, omission error is the number of validation pixels which are not classified for a land cover type while in real they belong to that land cover type (Jensen, 1986).

4. Results and Discussion

The combination of band 1, 2 and 3 in red, green and blue respectively proved to be essential for enhancement of land cover types (Fig. 2). The false colour composite image together with the geological map covering the study area (Robb et al., 2006), was used in the generation of training classes of six land cover types. These were used for the construction of land cover maps using

supervised classification algorithms (Fig. 4 (a)-(h)). As it can be observed in Table 5, with the exceptions of Spectral Angle Mapper and Spectral Information Divergence, all land cover maps attained overall accuracy in the range of 94-99%, which represent good classification (Aronoff, 1982), and Kappa coefficient values exceeding 0.9 which also indicate good classification (Altman, 1991). Support Vector Machine land cover map attained highest overall accuracy and Kappa coefficient value of 99% and 0.98, respectively.

Because of high overall accuracy and Kappa coefficient attained by most land cover maps (Fig. 4 (a)-(f)), it was important to report the accuracy of individual land cover types in the maps. All eight classification maps (Figure 4 (a)-(h)) provided higher producer's accuracy (>95 %) for forest (Table 5). However, only Support Vector Machine and Minimum Distance maps attained producer's accuracy in the range of 80-100% for all land cover types (Table 6). Spectral Information Divergence provided lowest producer's accuracy for vegetation, Duiwelskloof leucogranite and built-up land; while Spectral Angle Mapper attained lowest producer's accuracy for waterbody. Mahalanobis Distance acquired producer's accuracy of 3% for Turfloop granite which is the lowest value attained for this land cover type (Table 6). Producer's accuracy is an important parameter as it measures how well a certain land cover type has been classified (Jensen, 1986). Another important parameter of determining accuracy of individual land cover types is the user's accuracy which measures the reliability or precision of algorithm in classifying a land cover type when it is that land cover type (Jensen, 1986). This parameter estimates the level of confidence that can be attributed to pixels classified as belonging to a land cover type in a map. All eight land cover maps (Fig. 4 (a)-(h)) provided higher user's accuracy (>95%) for forest (Table 7). However, only Support Vector Machine, Minimum Distance and Neural Network land cover maps attained user's accuracy above 80% for all land cover types (Table 7).

Out of the six land cover maps (Fig. 4 (a)-(f)) that attained high overall accuracy and Kappa coefficient (Table 5), Mahalanobis Distance have lowest user's accuracy of <50% for Turfloop granite and built-up land. These two land cover types also show high commission and omission error in most land cover maps (Tables 8 and 9). This could be attributed to environmental conditions and distribution of built-up land and Turfloop granite in the area since there is spatial overlapping and lack of abrupt boundaries between the two land cover types (Fig. 2). The separability difficulty of Turfloop granite and built-up land was also observed during the examination of ROIs of the land cover types with the aid of n-D Visualizer (Table 3 and Fig. 3). Therefore, the high producer's and user's accuracy attained for forest, waterbody and vegetation by all classification algorithms can be attributed to their clear boundaries, which enable the algorithms to assign pixels to their corresponding land cover types with less misclassification error (Jensen, 1986). In general, Spectral Angle Mapper and Spectral Information Divergence performed poorly in classifying most land cover types especially the Turfloop granite and built-up land (Table 7). This supports the findings of previous study of Rajashekararadhya and Shivakumar (2017) which demonstrated that Spectral Angle Mapper and Spectral Information Divergence perform poorly in classification of land cover types without clear boundaries.

Table 5. Overall accuracy (%) and Kappa coefficient of algorithms.

Item	SVM	MD	MhD	ML	NN	Pp	SAM	SID
Overall accuracy	99.28	98.82	94.45	97.23	98.39	94.13	66.12	55.47
Kappa value	0.990	0.984	0.928	0.964	0.979	0.9248	0.5818	0.462

Table 6. Producer's accuracy (%) for land cover types.

Land cover type	SVM	MD	MhD	ML	NN	Pp	SAM	SID
Forest	100.00	100.00	99.97	100.00	99.19	98.60	100.00	99.94
Waterbody	100.00	100.00	99.90	99.90	99.90	99.95	63.19	73.66
Vegetation	100.00	100.00	100.00	99.84	100.00	99.98	99.96	54.14
D-leucogranite	100.00	98.83	98.43	98.07	99.52	88.99	7.68	0.44
T-granite	81.55	83.69	3.21	35.03	68.98	40.64	9.63	5.88
Built-up land	98.08	91.47	55.01	97.87	95.31	77.61	22.39	10.45

Table 7. User's accuracy (%) for land cover types.

Land cover type	SVM	MD	MhD	ML	NN	Pp	SAM	SID
Forest	100.00	100.00	100.00	100.00	99.94	100.00	100.00	99.26
Waterbody	99.95	100.00	99.18	100.00	99.37	100.00	63.19	61.23
Vegetation	99.92	98.50	99.01	100.00	99.88	90.33	99.96	85.79
D-leucogranite	99.76	99.96	99.35	99.84	97.83	99.28	18.04	10.09
T- granite	97.76	88.67	5.41	92.91	97.73	59.85	11.61	1.06
Built-up land	87.95	89.34	42.64	61.04	81.87	65.94	4.02	3.05

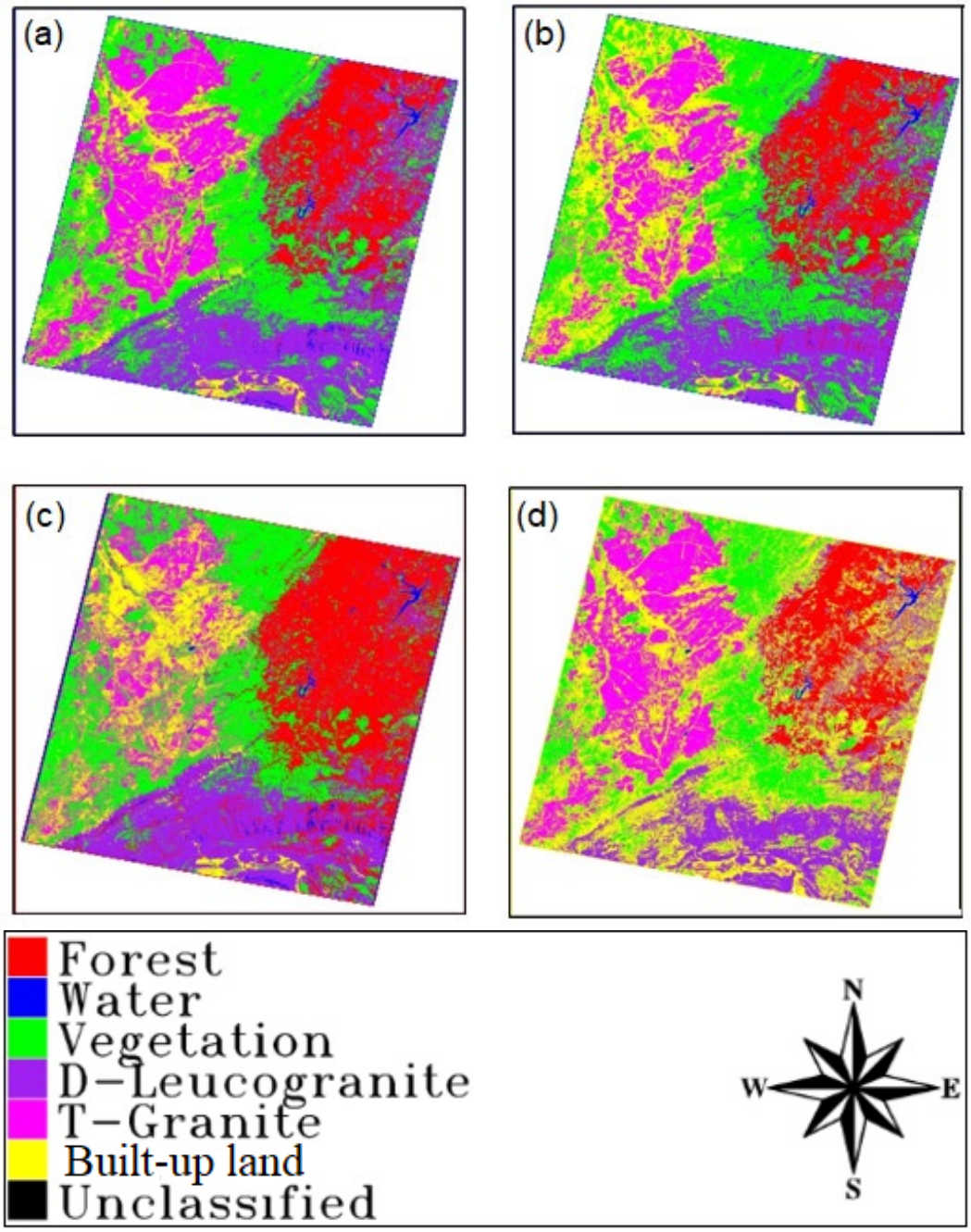

Figure 4 (a)-(d): Land cover maps generated using (a) Support Vector Machine, (b) Minimum Likelihood, (c) Neural Network and (d) Maximum Likelihood. (a) Support Vector Machine and (b) Minimum Likelihood, which attained relatively better individual accuracies for land cover types, are visually almost similar.

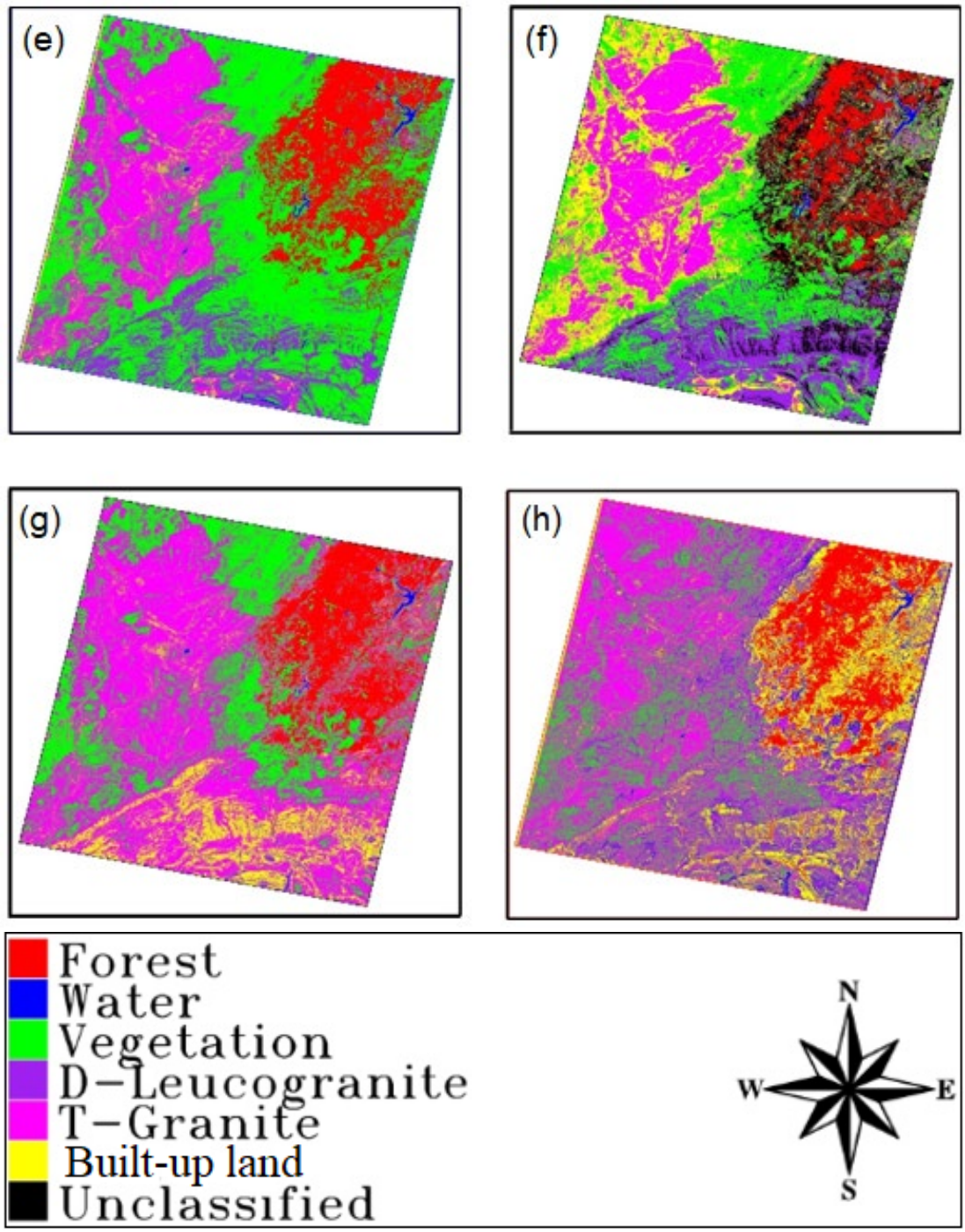

Figure 4 (e)-(h): Land cover maps generated using (e) Mahalanobis Distance, (f) Parallelepiped, (g) Spectral Angle Mapper and (h) Spectral Information Distance. It is visually evident that (h) Spectral Information Divergence attained highest misclassification error for most land cover types.

Table 8. Commission error (%) for land cover types.

Land cover type	SVM	MD	MhD	ML	NN	Pp	SAM	SID
Forest	0.00	0.00	0.00	0.00	0.06	0.00	0.00	0.74
Waterbody	0.05	0.00	0.82	0.00	0.63	0.00	7.42	38.77
Vegetation	0.08	1.50	0.99	0.00	0.12	9.67	0.04	14.21
D-leucogranite	0.24	0.04	0.65	0.16	2.17	0.72	81.96	89.91
T-granite	2.24	11.33	94.59	7.09	2.27	40.16	88.39	98.94
Built-up land	12.05	10.63	57.36	38.96	18.13	34.06	95.98	96.95

Table 9. Omission error (%) for land cover types.

Land cover type	SVM	MD	MhD	ML	NN	Pp	SAM	SID
Forest	0.00	0.00	0.03	0.00	0.81	1.40	0.00	0.06
Waterbody	0.00	0.00	0.10	0.10	0.10	0.05	36.81	26.34
Vegetation	0.00	0.00	0.00	0.16	0.00	0.12	0.04	45.86
D-leucogranite	0.04	1.17	1.57	1.93	0.48	11.01	92.32	99.56
T- granite	18.42	16.31	96.79	64.97	31.02	59.36	90.37	94.12
Built-up land	1.92	8.53	44.99	2.13	4.69	22.39	77.61	89.55

5. Conclusion

This study demonstrated the significance of band combination technique in generating false colour composite image to enhance land cover types that can be used to generate training classes for supervised classification. The generated training classes of six land cover types: waterbody, forest, vegetation, Duiwelskloof leucogranite, Turfloop granite and built-up land formed the basis of supervised classifications using eight algorithms. The eight classification maps were subjected to accuracy assessment (confusion matrix) to determine the effectiveness of the algorithms in correctly classifying the land cover types and level of confidence that can be attributed to their respective land cover maps. Support Vector Machine, Minimum Distance, Mahalanobis Distance, Maximum Likelihood, Neural Network and Parallelepiped land cover maps attained overall accuracy and Kappa coefficient beyond 90% and 0.9, respectively, which represent good classification. All land cover maps provided high producer's and user accuracy for land cover types with clear boundaries (forest, waterbody and vegetation). Meanwhile, most algorithms poorly performed in classifying spatially overlapping land cover types without abrupt boundaries (Turfloop granite and built-up land). Therefore, it can be concluded that environmental conditions and distribution of land cover types can affect the performance of classification algorithms. Also, it can be recommended to investigate the heterogeneity or homogeneity of a region prior to selection of suitable algorithms and to study the separability of land cover types to avoid misclassifications.

Support Vector Machine and Minimum Distance provided better producer's and user's accuracy, beyond 80%, for all land cover types. The producer's and user's accuracy are significant in determining precision of algorithm in classifying the land cover types and confidence level that can be attributed to the land cover classification maps. Therefore, the confidence level of beyond 80% can be attributed to the pixels classified for all land cover types in the Support Vector Machine and Minimum Distance land cover maps. In summary, the most effective supervised classification algorithms in the region based on the accuracy assessment are; (in decreasing order of effectiveness)

Support Vector Machine, Minimum Distance, Neural Network, Maximum Likelihood, Mahalanobis Distance and Parallelepiped. These algorithms can therefore be used to generate and update land cover maps for regions of similar environmental conditions; and special preference is given to algorithms that attained producer's and user's accuracy beyond 80% for all land cover types.

6. References

Altman, D.G., 1991, Practical statistics for medical research: London, Chapman and Hall.

Alrababah, M.A., and Alhamad, M.N., 2006, Land use/cover classification of arid and semi-arid Mediterranean landscapes using Landsat ETM: International Journal of Remote Sensing, v. 27, p. 2703-2718.

Aronoff, S., 1982, The map accuracy report-A user's view: Photogrammetric Engineering and Remote Sensing, v. 48(8), p. 1309-1312.

Bagan, H., Wang, Q., Watanabe, M., Kameyama, S., and Bao, Y., 2008, Land-cover classification using ASTER multi-band combinations based in wavelet fusion and SOM neutral network: American Society for Photogrammetry and Remote Sensing, v. 74(3), p. 333-342.

Comber, A.J., Fisher, P.F., and Wadsworth, R.A., 2005, What is land cover? Environment and planning: Planning and Design v. 32, p. 199-209.

Du, Y., Chang, C.I., Ren, H., D'Amico, F.M., and Jensen, J.O., 2004, New hyperspectral discrimination measure for spectral characterization: Optical Engineering, v. 43(8), p. 1777-1786.

Fuller, R.M., Groom, G.B., Mugisha, S., Ipulet, P., Pomeroy, D., Katende, A., Bailey, R., and Ogutu-Ohwayo, R., 1998, The integration of field survey and remote sensing for biodiversity assessment: A case study in the tropical forests and wetlands of Sango Bay, Uganda: Biological Conservation, v. 86, p. 379-391.

Green, A.A., and Craig, M.D., 1985, Analysis of aircraft spectrometer data, with logarithmic residuals: Proceedings of the Airborne Imaging Spectrometer Data Analysis Workshop, p. 111-119.

Hsu, C.W., Chang, C.C., and Lin, C.J., 2007, A practical guide to support vector classification: National Taiwan University, p. 1-16.

Jansen, L.J.M., Bagnoli, M., and Focacci, M., 2008, Analysis of land-cover/use change dynamic in Manica Province in Mozambique in a period of transition (1990-2004): Forest Ecology and Management, v. 254, p. 308-326.

Jensen, J.R., 1986, Introductory digital image processing: New Jersey, Englewood Cliffs, Prentice-Hall.

Lobo, A., Legendre, P., Rebollar, J.L.G., Carreras, J., and Ninot, J.M., 2004, Land cover classification at a regional scale in Iberia: Separability in a multi-temporal and multi-spectral data set of satellite images: International Journal of Remote Sensing, vol. 25(1), p. 205-213.

Kruse, F.A., Lefkoff, A.B., Boardman, J.B., Heidebrecht, K.B., Shapiro, A.T., Barloon, P.J., and Goetz, A.F.H., 1993, The Spectral Image Processing System (SIPS)-Interactive visualization and analysis of imaging spectrometer data: Remote Sensing of the Environment, v. 44, p. 145-163.

Mohd, H.I., Pakhriazad, H.Z., and Shahrin, M.F., 2009, Evaluating supervised and unsupervised techniques for land cover mapping using remote sensing data: Malaysian Journal of Society and Space, v. 5(1), p. 1-10.

Musaoglu, N., Coskun, M., and Kocabas, V., 2005, Land use change analysis of Beykoz- Istanbul by means of satellite images and GIS: Water Science and Technology, v. 51, p. 245-251.

NASA, 2013, Landsat 7 Science Data User's Handbook. Available at http://landsathandbook.gsfc.nasa.gov.

Rajashekararadhya, S.V., and Shivakumar, B.R., 2017, Performance analysis of Spectral Angle Mapper and Spectral Information Divergence classifiers; A case study using homogeneous and heterogeneous remotely sensed data: International Journal of Advanced Research in Electrical, Electronics and Instrumentation Engineering, v. 6(7), p. 5685-5692.

Research Systems Inc, 2008, ENVI Tutorials: Research Systems Inc, Boulder CO.

Richards, J.A., and Jia, X., 2006, Remote sensing digital image analysis, 4th edn: Berlin, Springer-Verlag.

Robb, L., Brandl, G., Anhaeusser, C.B., and Poujol, M., 2006, Archaean granitoid intrusions, in Johnson, M.R., Anhaeusser, C.R., and Thomas, R.J., eds., The Geology of South Africa: Pretoria, Geological Society of South Africa, p. 57-94.

Whateley, M.K.G., 2006, Remote sensing, in Moon, C.J., Whateley, M.K.G., and Evans, A.M., eds., Introduction to Mineral Exploration: Australia, Blackwell Publishing, p. 214-218.

Yuksel, A., Akay, A.E., and Gundogan, R., 2008, Using ASTER imagery in land use/cover classification of Eastern Mediterranean Landscapes according to CORINE land cover project: Sensors, v. 8, p. 1237-1251.